Stochastic Simulation of Activation in the G-Protein Cascade of Phototransduction

T. D. Lamb

Physiological Laboratory, University of Cambridge, Downing Street, Cambridge CB2 3EG, United Kingdom, and Division of Neuroscience, John Curtin School of Medical Research, Australian National University, Canberra, ACT 2601, Australia

ABSTRACT Activation of the G-protein cascade underlying phototransduction has been modeled by simulating the two-dimensional diffusional interactions that occur at the rod disc membrane between the three reacting protein species, which are the activated rhodopsin (R*), the G-protein (G), and the effector protein (E, the phosphodiesterase, PDE). The stochastic simulations confirm the main predictions of a simplified analytical model (Lamb, T. D., and E. N. Pugh, 1992, *Journal of Physiology* 449:719–758), and extend that treatment to more complicated cases, where there is a finite probability of reaction or a finite time for reaction. The simulations also provide quantitative estimates of the efficiency of coupling from activated G-protein (G*) to activated effector (E*) in terms of the concentrations, lateral diffusion coefficients, and binding rate constants of the participating molecules; the efficiency of coupling from G* to E* is found to be not as high as in the previous simplified analytical theory. The findings can be extended to other G-protein cascades, provided that the physical parameters of those cascades are specified.

INTRODUCTION

G-protein cascades mediate signal transduction in a wide variety of signaling systems, of which the photoreceptor is a prime example. In the general case, an activated receptor protein (R*) catalyzes the activation of a G-protein to G*, which in turn activates an effector protein to E* (see Fig. 1). Although the reactions of G-protein cascades have been understood in qualitative terms for a number of years, quantitative approaches have been lacking. Recently, we presented a simplified analytical description of the amplification and the rising phase kinetics of the G-protein cascade of vertebrate photoreceptors, in which we approximated the lateral diffusion of the molecules in the plane of the disc membrane by the diffusion of heat in two dimensions (Lamb and Pugh, 1992).

A surprising outcome of the approximate analysis was that, for the activation of E* by G*, the "coupling efficiency" (defined below) was predicted to be quite close to unity, even when the membrane concentration of effector protein was far lower than the concentration of G-protein. With parameters appropriate to the photoreceptor disc membrane, we predicted that the coupling efficiency from G* to E* could approach 90%, even when the ratio of effector to G-protein concentration in the membrane was as little as 1:10.

Both to test that prediction, and to extend the analysis to include parameters that could not be considered in the simplified model, the G-protein cascade of phototransduction has now been simulated as a stochastic process involving

two-dimensional diffusion of the protein molecules in the plane of the disc membrane. The simulations confirm the general form of the predictions from the simpler analytical model, although they show that the coupling efficiency is not as high as previously predicted, and they permit investigation of the effects of finite reaction probability and finite reaction time on the kinetics of the cascade. A preliminary report of these findings has been presented (Lamb, 1993).

THE G-PROTEIN CASCADE

Details of the molecular interactions underlying phototransduction have been reviewed recently (Pugh and Lamb, 1993; Hofmann and Heck, 1994), and the reactions important to activation of the G-protein cascade are indicated schematically in Fig. 1. Activation of the cascade can be divided conceptually into two phases. 1) An activated receptor protein, R* (activated rhodopsin, in the case of the photoreceptor) catalytically activates numerous molecules of the G-protein to G*. 2) Each activated molecule of G* must then bind to a molecule of effector protein, to activate it to E*. The diffusional nature of these steps is sketched in Fig. 1 B. A single molecule of R* diffuses laterally in the disc membrane, sequentially encountering and activating molecules of G, which are themselves also diffusing laterally in the membrane. In the second step the diffusing G* molecules, which will have been produced at different locations and times according to the trajectory of the single R* molecule, must locate and bind to molecules of effector E.

Diffusion-limited activation

The diffusion limit to the rate of activation occurs when each molecular contact (of the appropriate species) leads to reaction, on every occasion and with no delay. Our previous analytical consideration was further restricted to the case of
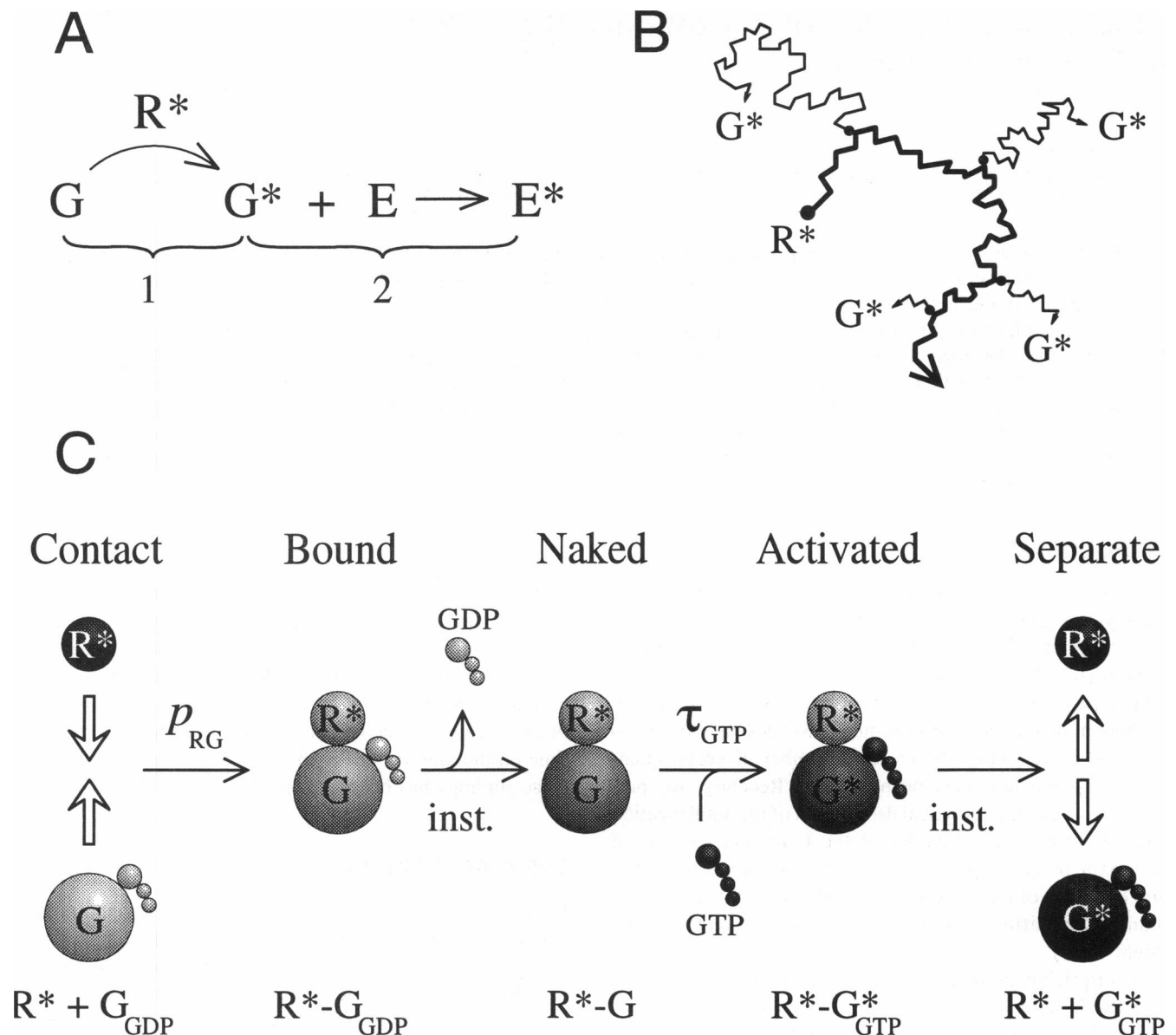
FIGURE 1   The reactions of the G-protein cascade. (A) Overall reaction. In the first phase, a molecule of R* catalyzes the activation of the G-protein from G to G*; in the second phase, G* binds to the inactive form of the effector protein E, to create the active form E*. (B) Sketch of the diffusional nature of the activation of G*. The heavy trace represents the path followed by a single active R*, diffusing within a sea of molecules of G (which are not shown). The R* collides with molecules of G, and activates some of them to G*. The thin traces represent the paths followed by the G*s after their activation. (C) Microsteps involved in the activation of G*. When the R* comes into contact with an inactive G ($= G_{GDP}$), there is some probability p_{RG} (see text) that the two will bind to form R^*-G_{GDP}. The GDP then rapidly dissociates, and after some random interval with a mean of τ_{GTP}, a GTP is taken up from the cytoplasm to form the activated complex, $R^*-G^*_{GTP}$. The two protein components then rapidly separate, to form G* ($= G^*_{GTP}$) together with the unaltered R*, which is free to repeat the cycle.

pure activation (i.e., all inactivation reactions were ignored), to render the mathematics tractable, and because the inactivation reactions remain poorly understood (see Pugh and Lamb, 1993; Hofmann and Heck, 1994). In this paper the stochastic simulations are similarly restricted to the activation steps, but in the future it will be straightforward to introduce inactivation reactions as soon as the molecular details and rate constants have been determined.

An analytical treatment of the first reaction step is relatively straightforward in the diffusion limit. Lamb and Pugh (1992) determined the average behavior using the approach of Razi Naqvi (1974), who applied the solution given by

Jaeger (1942) for an analogous problem in the two-dimensional diffusion of heat. That solution is given below in Eq. 3, and is compared with the results of the stochastic simulations. To a reasonable approximation, a single molecule of R* causes activation of G* at a nearly constant rate (i.e., the quantity of G* approximately ramps with time after activation of one R*), and the slope can be expressed in terms of the concentration of G-protein and the lateral diffusion coefficients.

An analytical treatment of the second step, the coupling from G* to E*, is made very difficult by the fact that the spatial distribution of G* is not readily expressible, inasmuch

as it depends upon the particular trajectory of a single R* molecule. Nevertheless, an approximate solution for the coupling was found by Lamb and Pugh (1992), and the time course of E* activation was predicted also to ramp with time, but at a lower rate than for G*. The ratio of the E* activation rate to the G* activation rate was defined as the coupling efficiency, c_{GE}, of the reaction from G* to E*. A revised expression for the coupling efficiency is given below in Eq. 9, and the predictions are compared with the results of the stochastic simulations.

Microsteps in the activation of G*

For a more realistic analysis of activation in the cascade, it is necessary to go beyond the diffusion-limited case to consider the reactions underlying the catalysis of G*. R* catalyzes the replacement of a GDP by a GTP at a binding site on the G-protein, to give the active form $G*_{GTP}$. The overall reaction may be written as $G_{GDP} + GTP \rightarrow G*_{GTP} + GDP$; the underlying microsteps are shown in Fig. 1 C. A molecular description of these microsteps has been given by Hofmann and Kahlert (1992).

Upon contact between an R* and an inactive G (= G_{GDP}), there is some probability p_{RG} (see below) that the two will bind, to form R*—G_{GDP}. The GDP rapidly dissociates from this bound complex to leave the naked R*—G complex. After a finite mean delay time τ_{GTP}, a molecule of GTP will be taken up, forming the activated complex R*—$G*_{GTP}$. The actual delay time on any occasion will be stochastic, and the rate constant k_{GTP} of the step will equal τ_{GTP}^{-1}; this rate constant is expected to increase linearly with the cytoplasmic concentration of GTP, at least at low concentrations. The activated complex R*—$G*_{GTP}$ is unstable and rapidly dissociates to form the activated G-protein, $G*_{GTP}$, together with the unaltered R*. This R* is then available to catalyze the activation of further molecules of G.

The $G*_{GTP}$ is generally thought to split into its α and $\beta\gamma$ subunits, with the α-subunit representing the activated form G*, although Heck and Hofmann (1993) have recently suggested that G* in fact corresponds to the holomeric form. The rate of cycling by R* will not, however, be affected by whether such splitting occurs; the most that a splitting step could do would be to introduce a delay into the subsequent activation of E*. In the simulations, splitting of the α and $\beta\gamma$ subunits will be assumed to occur instantaneously. In addition, to minimize the number of parameters, the dissociation of GDP from the bound complex, and the separation of R* from G*, will be taken to occur instantaneously (see Fig.1 C). Thus the catalysis of G to G* will be taken to involve 1) diffusional contact between the R* and a G, 2) a finite probability p_{RG} of R*:G binding, and 3) a stochastic reaction time with a mean of τ_{GTP}. In the diffusion limit, the R*:G binding rate constant k_{RG} (corresponding to p_{RG}, see below) approaches infinity, and τ_{GTP} is 0.

Activation of E*

The activation of E* involves diffusional contact between G* and the inactive effector, E. In the case of the phototrans-

duction cascade, a complication is that the phosphodiesterase molecule actually comprises two catalytic components: two nearly identical subunits (α and β) are each enzymatically active, and each has an inhibitory γ-subunit that can bind G*. As discussed by Pugh and Lamb (1993), the available evidence suggests that the two catalytic components behave more or less independently. Therefore, to avoid complication and to maintain comparability of treatment between different G-protein cascades, the effector E will be represented as a single enzymatic component. In the case of the photoreceptor, the concentration C_E of effector subunits E will be double that of the holomeric phosphodiesterase (PDE), and the enzymatic activity will be half that of the fully activated PDE. Thus the additional reaction G* + E* $\rightarrow$ E**, which occurs only in photoreceptors, will be accommodated simply by doubling the number of particles of effector.

The only parameter needed to specify the reaction of G* with E is the probability p_{GE} (or rate constant k_{GE}) that diffusional contact between G* and E leads to their binding, to form G*—E (= E*).

THEORY

Activation of G* in the continuous model

A theoretical expression for the diffusion-limited rate of activation of G* was derived by Lamb and Pugh (1992) in their Eq. A1. Here that expression is generalized to nondiffusion-limited cases, by considering a finite rate constant of binding of R* to G, and by introducing a finite GTP binding time, τ_{GTP}. Whereas conceptually it may be easiest to view the binding of R* to G as occurring with some probability p_{RG} upon collision (see Fig. 1 C), this probability actually applies over a finite interval, such as the simulation time step Δt, and in the continuous case the binding is more appropriately specified in terms of a rate constant k_{RG} (defined subsequently). The diffusion limit to the rate of activation of G* in the continuous model occurs when k_{RG} is infinite and τ_{GTP} is 0.

An expression is required for the rate at which a single molecule of R* activates molecules of G, when the two molecular species undergo diffusion, with lateral diffusion coefficients D_{R*} and D_G. As discussed by Razi Naqvi (1974) and Lamb and Pugh (1992), this problem is mathematically equivalent to the case of a stationary R* reacting with diffusing molecules of G, which move with an effective lateral diffusion coefficient $D_{R*} + D_G$. The molecules of G are considered as infinitesimal points, whereas the immobile R* is assigned an effective collision radius equal to the sum of the two molecular radii, $\rho_{RG} = \rho_{R*} + \rho_G$. This problem is in turn equivalent to the two-dimensional diffusion of heat into a sink at internal radius ρ, and has been solved by Jaeger (1942).

The symbol $c_G(r, t)$ will denote the concentration of inactive G-protein remaining at radius r and time t, from an initial uniform level of C_G, and $\nu_G(t)$ will denote the rate of activation of G* by a single R* formed at the origin at time 0. For simplicity, subscripts will be dropped unless needed to avoid ambiguity; thus $c = c_G(r, t)$, $C = C_G$, $\nu = \nu_G(t)$,

$k = k_{RG}$, $\rho = \rho_{RG}$ and $D = D_{R^*} + D_G$; the concentration $c_G(\rho, t)$ at the collision radius ρ will be denoted c_ρ.

The rate ν of activation of G* is equal to the rate of removal of G, and may be expressed in terms of the flux of inactive G at the collision radius ρ as

$$\nu = k(\pi\rho^2)c_\rho, \tag{1a}$$

$$= (2\pi\rho)D\partial c/\partial r|_\rho. \tag{1b}$$

Eq. 1a expresses the rate of reaction at the collision radius, whereas Eq. 1b expresses the rate of diffusion of G into the region. Together Eqs. 1a and 1b express the boundary condition for the diffusion equation, at $r = \rho$. k has dimensions of time^{-1} and represents the rate constant of destruction of G, when the concentration c is taken as uniform over the area $\pi\rho^2$ at a value of $c = c_\rho$.

For this boundary condition, and with initial condition $c = C$, the solution derived by Jaeger (1942) for the concentration c_ρ at the collision radius ρ is

$$c_\rho = C\, I(a, \alpha) \tag{2}$$

where the function $I(a, \alpha)$ has been defined and tabulated by Jaeger, and where $a = k\,\rho^2/2D$ and $\alpha = Dt/\rho^2$. The rate ν is then obtained by substitution of Eq. 2 into Eq. 1a, as $\nu = k(\pi\rho^2)CI(a, \alpha)$. Given that $I(a, 0) = 1$, the initial rate ν_0 at very early times remains finite when k is finite, at a value of $\nu_0 = k(\pi\rho^2)C$.

Expansion of the function $I(a, \alpha)$, according to Eq. 16 of Jaeger (1942), gives the solution for the rate of activation of G* as

$$\nu = 4\pi DC\{z^{-1} - \gamma z^{-2} - (\pi^2/6 - \gamma^2)z^{-3} + \cdots\} \tag{3a}$$

where

$$z = 4D/k\rho^2 + \ln 4Dt/\rho^2 - 2\gamma, \tag{3b}$$

and $\gamma \approx 0.57722$ is Euler's constant. The total quantity of G*, denoted $G^*(t)$, is given by the time integral of the rate ν in Eq. 3a.

The factor $4D/k\rho^2$ ($= 2/a$) in Eq. 3b mediates the effect of the R*:G binding reaction. For $k = \infty$, this factor is 0, and the equation gives the diffusion limit to the rate of activation. (In this case Eq. 3 reduces to Eq. A1 of Lamb and Pugh (1992), if only the first term in the expansion { } is taken). For k small, the factor $4D/k\rho^2$ dominates Eq. 3b so that z is very weakly dependent on time, and ν is therefore nearly constant. Thus, if the reaction is far from the diffusion limit because of k being small, then the time course of $G^*(t)$ is very close to a ramp.

Finite time for GTP binding

To account for a finite mean time τ_{GTP} for binding of GTP to R*—G, it is helpful first to consider the limit to the rate of activation of G* when τ_{GTP} becomes large. When this occurs, the rate of activation ν will approach the reciprocal of τ_{GTP}, termed the rate constant of GTP binding, $k_{GTP} = \tau_{GTP}^{-1}$. Thus if τ_{GTP} were 1 ms, then ν would be close to 1000

G* s^{-1} (for a single R*). Hence when τ_{GTP} is large, $G^*(t)$ will ramp in time with a slope of k_{GTP}.

The expression required for ν therefore has a limit of k_{GTP} when τ_{GTP} is large, and a limit given by Eqs 3a and 3b when τ_{GTP} approaches 0. I have not been able to derive such an expression on purely theoretical grounds, but I found it possible to obtain a very good match to the simulations, as well as the correct limiting behavior, with the expression

$$\nu = [\nu_{diff}^{-b} + k_{GTP}^{-b}]^{-1/b} \tag{3c}$$

where ν_{diff} represents the rate predicted by Eq. 3a, and where an exponent of $b \approx 1.5$ provided the best fit to the simulations. Eq. 3c represents a kind of weighted average of the rates of reaction due to diffusion and due to GTP binding.

Diffusion and reaction on a square lattice

In this paper lateral diffusion of molecules and the reactions between molecules will be simulated in terms of a discrete square-grid lattice. For a previous simulation of the diffusion-limited catalytic activation reaction in two dimensions (i.e., the first step in the cascade), see Torney et al. (1987). The purpose of this and the following section is to relate the parameters of the continuous model to those of the square lattice approximation.

In the continuous case, the expected mean-square distance $\langle r^2 \rangle$ traversed by a molecule diffusing in two dimensions is given by

$$\langle r^2 \rangle = 4Dt \tag{4}$$

where D is the molecule's lateral diffusion coefficient, and t is time (see, e.g., Berg, 1983). In a square lattice with spacing Δx, and for a time increment Δt, the simulated diffusion coefficient may be shown to be given by

$$D = \frac{(\Delta x)^2}{4\Delta t} p_{move} = D_{max}p_{move} \tag{5}$$

in the case where each molecule is able to move to any one of the four nearest orthogonal locations on the lattice, and where p_{move} is the probability that the molecule moves in each interval Δt. Thus the maximum diffusion coefficient that can be simulated under these conditions is $D_{max} = \frac{1}{4}(\Delta x)^2/\Delta t$.

In the continuous model, two molecules of circular cross-section come into contact when the distance between their centers equals the collision radius ρ, given by the sum of their molecular radii, e.g., $\rho_{RG} = \rho_{R^*} + \rho_G$. In the square lattice, the simplest notion of "contact" is when the second molecule occupies one of the four orthogonal locations nearest the first molecule; this is comparable to the case above for the permitted molecular movements in the simulation of diffusion. However, given that the molecules are only able to move in discrete increments and at discrete intervals rather than in a continuum, and that the lattice spacing Δx may not equal ρ, this is not necessarily the most appropriate representation of contact. It is possible instead to assign any arbitrary combination of the eight lattice points surrounding a molecule as
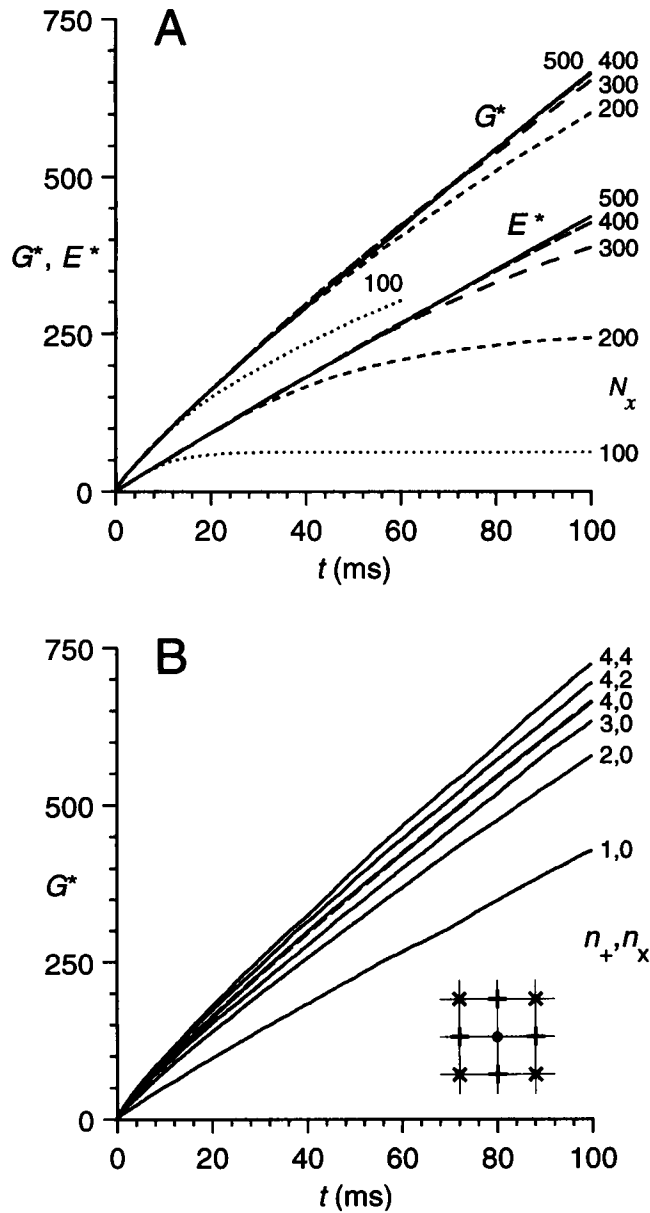
FIGURE 2 Determination of appropriate values for the lattice size and the contacting locations in the square lattice simulations. Except where otherwise stated, all traces were obtained with the standard simulation parameters in Table 1. (A) Finite lattice size. The upper traces plot $G^*(t)$, and the lower traces plot $E^*(t)$, for square lattices of the indicated sizes of $N_x \times N_x$ pixels. For $G^*(t)$ there is no significant difference between the simulations with N_x equal to 400 or 500, although for $E^*(t)$ the simulation with $N_x = 400$ is marginally smaller than for $N_x = 500$. (B) Number of contacting locations. The simulated $G^*(t)$ responses are plotted for the indicated combinations of locations defined as "contacting" for the purposes of binding of the molecules (see Text). As indicated in the inset, n_+ and $n_\times$ are the numbers of orthogonal and diagonal locations at which contact is defined to be possible. Thus, for $n_+ = 4$ and $n_\times = 0$, a molecule of G can bind to an R* if and only if the G occupies one of the four locations immediately adjacent to the R*. The broken trace plots the diffusion limit for $G^*(t)$ in the continuous model, calculated from Eq. 3 with $k_{RG} = \infty$ and $\tau_{GTP} = 0$, and with collision radius $\rho_{RG} = 4.5$ nm; this trace virtually superimposes on the simulation for $n_+ = 4$ and $n_\times = 0$. The simulated traces were averaged from at least 50 repetitions in (A) and from at least 20 repetitions in (B).

being positions of contact for the purposes of binding; see inset to Fig. 2 B. The number of such "contacting" locations will be denoted $n_{contact}$, with n_+ in the orthogonal directions and $n_\times$ in the diagonal directions.

Equivalence of parameters between continuous and lattice models

The square lattice and the continuous case cannot be made precisely equivalent to each other because of their different geometries: in one case the collision boundary is square, whereas in the other it is circular. However, for the range of parameters considered in this paper, the equivalence appears to be very close. It was found that at very low rates of binding ($k \to 0$) the parameter $2/a$ in Eq. 3b was given by $(n_{contact}/4)$ p_{move}/p_{RG} (see Fig. 4), and that at very high rates of binding ($k \to \infty$) the effective collision radius varied approximately as $\pi\rho^2 = n_{contact}(\Delta x)^2$ (see Fig. 2 B). When the number $n_{contact}$ of "contacting" locations was restricted to the four orthogonal positions (so that $n_\times = 0$, and $n_+ = 4 = n_{contact}$), it was found that the best description of the behavior of the square lattice was given by the following interrelations:

$$\pi\rho^2 = 4(\Delta x)^2, \tag{6}$$

$$k_{RG} = (\pi/4)p_{RG}\,(1 + p_{move}p_{RG})\,\Delta t^{-1}, \quad p_{RG} \le 1 \tag{7}$$

so that the parameter $4D/k\,\rho^2\,(= 2/a)$ that appears in Eq. 3b becomes

$$4D/k\rho^2 = p_{move}/p_{RG}(1 + p_{move}p_{RG}). \tag{8}$$

In these equations p_{move} refers to the sum of the probabilities of movement of the two species, $p_{move} = p_{move,\,R^*} + p_{move,\,G}$, corresponding to the fact that $D = D_{R^*} + D_G$ in the continuous case. To a first approximation the parameters in Eqs. 6–8 simplify to: $\rho \approx \Delta x$, $k \approx p_{RG}/\Delta t$ and $2/a \approx p_{move}/p_{RG}$. The term $(1 + p_{move}\,p_{RG})$ is a correction factor that was found to be needed when both p_{move} and p_{RG} become large; this occurs when the simulation time step Δt is larger than ideally it should be. Fig. 4 illustrates the predictions of Eq. 3, using the values of ρ and $4D/k\rho^2$ obtained from Eqs. 6 and 8.

Coupling from G* to E*

For the subsequent reaction of G* with E, it seems reasonable to assume that expressions for ρ_{GE} and k_{GE} analogous to those in Eqs. 6 and 7 will be applicable. In the previous analysis of Lamb and Pugh (1992), a highly simplified approach gave a rough estimate for the efficiency of coupling from G* activation to E* activation; this coupling efficiency c_{GE} was defined as $c_{GE} = \nu_E/\nu_G$, where ν_E and ν_G are the average rates of activation of E* and G*. The prediction obtained previously was that, in the diffusion limit,

$$c_{GE} = \exp(-q) \tag{9a}$$

where q satisfies

$$E_1(q) = 4\pi D_{eff}C_E/\nu_G \tag{9b}$$

and where $E_1(q)$ is the exponential integral. In that formulation, the effective lateral diffusion coefficient D_{eff} was taken to be

$$D_{eff} = D_{R*} + D_{G*} + D_E. \qquad (9c)$$

In the present simulations the shape of the coupling relation, as a function of effector concentration C_E, is found to be accurately predicted by Eqs. 9a–c (Fig. 7), but the relation is shifted along the concentration axis by a factor of about two. In addition the three lateral diffusion coefficients are found not to be equally effective in contributing to the coupling (Fig. 8). To account for these findings, the effective lateral diffusion coefficient D_{eff} in Eq. 9c is here replaced by the weighted form

$$D_{eff} = w_{R*}.D_{R*} + w_{G*}.D_{G*} + w_E D_E \qquad (9d)$$

where w_{R*}, w_{G*} and w_E are weighting coefficients determined by fitting the results in Figs. 7 and 8.

METHODS

The reactions of the G-protein cascade were simulated numerically using random walk techniques. The computer program "WALK" was written in FORTRAN 77 and compiled with Microsoft 32-bit Fortran PowerStation. The program is available by anonymous FTP from the Biophysics Internet Server, and may be found in the directory "Computer_Programs" (see footnote at beginning of this article). Minimum requirements are a 486 processor with 6 MB RAM, running MS-DOS.

A region of disc membrane was represented by a square lattice with nonabsorbing boundaries. For purposes of visual demonstration, the program allows the protein molecules to be represented as multipixel circular regions, but for the calculations presented in this paper each molecule was represented by a single pixel on the lattice. The full set of standard simulation parameters is given in Table 1. The standard lattice was 400×400 pixels with lattice spacing $\Delta x = 5$ nm, giving a region 2 μm square, and the simulation step time was $\Delta t = 2.5$ μs. The rationale for the choice of these and other parameters is given below. During a single time step in the simulation, each molecule was allowed to diffuse, and thereafter each molecule of R* and G* was tested to determine whether a reaction should occur.

Simulation of lateral diffusion

Lateral diffusion of molecules was simulated using a pseudorandom number generator to determine whether, and where, a molecule should move. Given the probability of movement p_{move} ($= D/D_{max}$) of the molecule (see Eq. 5) and a random number x uniformly distributed in the interval 0–1, the factor $dirn = 4x/p_{move}$ was calculated. If $dirn$ was less than 4 then the molecule was moved a single lattice position in one

TABLE 1 Standard parameters for simulation of phototransduction in amphibian rods at 22°C

Symbol	Value	Units	Definition	
		Phototransduction: protein concentrations and lateral diffusion coefficients		
C_G	2,500	μm^{-2}	Concentration of G-protein in membrane	
C_E	250	μm^{-2}	Concentration of effector protein in membrane[‡]	
D_{R*}	0.7	μm^2 s^{-1}	Lateral diffusion coefficient of R*	
D_G	1.2	μm^2 s^{-1}	Lateral diffusion coefficient of G	
D_{G*}	1.5	μm^2 s^{-1}	Lateral diffusion coefficient of G*	
D_E	0.8	μm^2 s^{-1}	Lateral diffusion coefficient of E	
		Simulation: lattice and time parameters		
N_x	400		Number of lattice points (in each dimension)	
Δx	5	nm	Lattice spacing	
Δt	2.5	μs	Time increment	
t_{max}	100	ms	Maximum time of simulation	
		Simulation: dependent parameters		
L	2	μm	Lattice width and height;	$= N_x \Delta x$
N_G	10,000		Initial number of molecules of G:	$= L^2 C_G$
N_E	1,000		Initial number of molecules of E;	$= L^2 C_E$
f_{tot}	0.069		Fractional lattice occupancy;	$= (N_G+N_E)/N_x^2$
N_t	40,000		Number of time increments;	$= t_{max}/\Delta t$
D_{max}	2.5	μm^2 s^{-1}	Maximum lateral diffusion coefficient;	$= \frac{1}{4}(\Delta x)^2/\Delta t$
		Reaction parameters: diffusion limit		
p_{RG}	1		Probability R* and G bind upon collision[§]	see Eq. 7
τ_{GTP}	0	μs	Mean time for a GTP to bind to R*—G[¶]	$= k_{GTP}^{-1}$
p_{GE}	1		Probability G* and E bind upon collision[§]	as Eq. 7
$n_+, n_\times$	4, 0		Number of pixels where "contact" occurs	

[‡] For the photoreceptor, the concentration C_E of effector protein subunits is double the concentration C_{PDE} of the holo-PDE, which contains two catalytic subunits; see section titled Activation of E*.

[§] The probabilities p_{RG} and p_{GE}, for the binding of R* to G, and G* to E, apply over the simulation time increment Δt. These reactions may alternatively be specified, in terms independent of the simulation, by reaction rate constants k_{RG} and k_{GE} (see Eq. 7).

[¶] When a finite time for GTP binding was introduced ($\tau_{GTP} > 0$), as in Fig. 5, it was necessary to specify the lateral diffusion coefficient of the molecular species R*—G; this was set to $D_{R*—G} = 0.4$ μm^2 s^{-1}. This parameter is not needed when $\tau_{GTP} = 0$, because the species spends no time diffusing.

of the four orthogonal directions, according to the value of INT(*dirn*) + 1; otherwise the molecule was not moved.

A difficulty arises when the molecule would have moved into an occupied position. The simplest solution is not to let the molecule move on that occasion, but this leads to a significant reduction in the simulated diffusion coefficient in cases where the fraction of occupied lattice positions, f_{tot}, is appreciable; for the standard conditions the error was typically 10%. It was found that a substantial improvement could be obtained by randomly trying further directions until a vacant position was found. Nevertheless, when the fractional occupancy of the lattice was appreciable, a residual reduction in effective diffusion coefficient remained (see following test). Except in early simulations, a correction was made to p_{move} to minimize this error.

To test the accuracy of the diffusion algorithm under the standard simulation conditions, the mean square distance traveled by molecules was compared with theory. A random initial distribution of molecules of G and E was allowed to diffuse in the absence of any R*, so that no reactions occurred. The initial positions of the molecules in a central region of interest, and the final positions of the same molecules at the end of the simulation, were recorded. Then, for the two species of molecule, the average of the mean square distances traveled was calculated and compared with Eq. 4. To provide a clear distance, *l*, from the boundary of at least 1 μm (200 pixels), the lattice was extended to 600 × 600 pixels in this test, and only molecules initially within the central 200 × 200 pixel region were monitored. To allow a fair comparison with theory, it was necessary to restrict the expected $\langle r^2 \rangle$ to be considerably smaller than the square of the clear distance available for diffusion, i.e., $4 D t_{max} \ll l^2$. Thus the simulation time was restricted to $t_{max} = 10$ ms, and all other parameters were set to the standard values in Table 1. With D_G and D_E equal to 1.2 and 0.8 μm^2 s^{-1}, this gave an expected $\langle r^2 \rangle$ of 0.048 and 0.032 μm^2 for G and E, respectively.

When the concentration of molecules was low (e.g., $C_G = C_E = 250$ μm^{-2}, corresponding to a fractional lattice occupancy of $f_{tot} = 1.25\%$), the values of $\langle r^2 \rangle$ obtained by the simulation were within 1% of the expected values. However, when the concentration of the G-protein was increased to its standard value of $C_G = 2500$ μm^{-2}, taking the fractional occupancy to $f_{tot} = 6.9\%$, the values of $\langle r^2 \rangle$ were low by a little over 3%, i.e., by roughly $\frac{1}{2} f_{tot}$. Therefore the probability of movement was increased slightly to correct for this effect: p_{move} was increased by $\frac{1}{2} f_{tot}$ (*ca* 3%, in the standard case). With this correction the simulated values of $\langle r^2 \rangle$ were found to be in extremely close agreement with theory.

Lattice spacing

The lattice spacing was chosen so as to provide a round number close to the collision radii of the reacting molecules. The diameters of rhodopsin, the G-protein, and the PDE are believed to be approximately 3, 6, and 7 nm, respectively (see Lamb and Pugh, 1992), giving a collision radius for the re-

action between R* and G of ρ_{RG} (= $\rho_{R^*} + \rho_G$) ≈ 4.5 nm, and for the reaction between G* and E of ρ_{GE} ≈ 6.5 nm. Hence Δx was chosen as 5 nm.

Lattice size

It is inevitable that the finite extent of the lattice will affect the accuracy of the simulations at longer times. To help minimize such edge effects, all the simulations in this paper began with the single R* placed at the center of the lattice.

The effect of lattice size is investigated in Fig. 2 *A*. The curves plot the average time course of activation of G* (upper set of curves) and of E* (lower set), for square lattices with the indicated number N_x of pixels in each dimension. All other parameters were held constant at the standard values (see Table 1). The finite lattice extent imposes a limitation at earlier times for the activation of E* than for the activation of G*, because of the lower density of effector protein in comparison with G-protein.

Although a lattice size of 200 × 200 pixels (1 μm square) is adequate for simulations to 25 ms, it is necessary to use a lattice of 400 × 400 pixels to avoid significant edge effects at times out to 100 ms. Even with this size it appears that the simulation for E* falls slightly below that obtained with a lattice of 500 × 500 pixels (2.5 μm square). However, because the activation of G* is not noticeably affected, and to obtain acceptable computation times, it was decided to standardize on a lattice size of 400 × 400 pixels (2 μm square).

Time increment

The time increment in the simulations must be set sufficiently small so that the probability of movement (p_{move}) of the most mobile molecular species is smaller than unity. From Eq. 5 the maximum diffusion coefficient that can be simulated is given by $D_{max} = \frac{1}{4} (\Delta x)^2 / \Delta t$. Because the most mobile species (G*) requires a lateral diffusion coefficient of $D_{G^*} = 1.5$ μm^2 s^{-1} (see Table 1), Δt must be kept less than about 4 μs for $\Delta x = 5$ nm. In fact, the value of Δt should be made as small as possible to maximize the effective rate constant of binding k_{RG} (see Eq. 7); this, however, will increase the computation time roughly in inverse proportion to Δt. As a compromise Δt was set to 2.5 μs for the standard case, giving $D_{max} = 2.5$ μm^2 s^{-1} and $p_{move, G^*} = 60\%$ for G*, and giving $k_{RG} \approx 500$ k s^{-1} when $p_{RG} = 1$. The effect of reducing Δt fivefold, to 0.5 μs, was to increase the computation time by about fourfold, but the consequent increase in k_{RG} resulted in only a few percent increase in the simulated rate of activation of G*.

Number of "contacting" locations

The effect of altering the number $n_{contact}$ of neighboring locations assigned as "contacting," in the sense defined earlier, is illustrated in Fig. 2 *B* for the activation of G* by R*. The annotations near the traces indicate the numbers of orthogonal (n_+) and diagonal ($n_\times$) positions defined as contacting.

The broken trace plots the analytical theory of Eq. 3, for the diffusion-limited continuous case (i.e., with k_{RG} and k_{GTP} infinite) and with $\rho_{RG} = 4.5$ nm. This curve is virtually indistinguishable from the simulated trace for $n_{contact} = 4$ ($n_+ = 4$, $n_\times = 0$).

The effect of altering the number of contacting locations in the square lattice appears equivalent to the effect of altering the collision radius ρ_{RG} in the continuous model. The traces in Fig. 2 B are in fact quite well described by Eq. 3 with ρ_{RG} and $2/a$ given by more complicated forms of Eqs. 6 and 8 that take into account the arrangement of contacting locations; curves not shown. The interpretation of the results in Fig. 2 B is that, although the precise number of locations defined as contacting is not critical, the best fit of the square lattice simulation (with $p_{RG} = 1$) to the diffusion-limited continuous case is obtained when the contacting locations are defined as the four orthogonal ones.

In early simulations, before the introduction of a correction to p_{move} (see section titled Simulation of Lateral Diffusion), when the simulated diffusion coefficients were reduced by a few percent, a similar match to the diffusion-limited continuous case was obtained by increasing the number of pixels defined as contacting to seven; i.e., with $n_+ = 4$, $n_\times = 3$. Those simulations are used only in Figs. 7 and 8.

Variance

For simulations repeated many times (e.g., ≥ 50 repetitions) a reasonable estimate of the ensemble variance could be obtained. It was found that the variance of the number of molecules produced had a similar time course to the mean number produced, and a broadly similar amplitude; thus, $\sigma^2(t) \approx \mu(t)$, as one might expect intuitively for a stochastic scheme of this kind. However, the equivalence did not seem to be exact. For conditions approaching the diffusion limit ($p_{RG} \approx 1$, $\tau_{GTP} \approx 0$) the variance of $G^*(t)$ was usually a little larger than the mean, whereas for conditions well below the diffusion limit ($p_{RG} \ll 1$, or $\tau_{GTP} \gg 0$) the variance of $G^*(t)$ may have been a little smaller than the mean. It is not clear whether this behavior represents statistical variation due to the limited number of repetitions, whether it represents a shortcoming in the simulations, or whether it is to be expected theoretically.

Computation time

For the standard parameters (a 400 $\times$ 400 lattice containing 11,000 molecules, and with $\Delta t = 2.5$ μs) a single simulation to $t_{max} = 100$ ms required more than 4×10^8 calls to the random number generator routine, and took approximately 1.5 h on a 486DX 33 MHz processor. All simulations were repeated at least 20 times, and a few were repeated 100 times (taking about a week).

Shortcut: creation of G* without G

A major factor extending the computation time is the large number of molecules of inactive G-protein: 10,000 Gs on the 2 μm $\times$ 2 μm region, for a standard G-protein concentration of $C_G = 2500$ μm^{-2}. An order of magnitude increase in speed can be obtained by doing away with these molecules of G, and simply allowing G*s to be created at the location of the R*, in a stochastic fashion and at some specified mean rate; this leaves 1000 molecules of E dominating the computation time. Activation of G* under these conditions closely approximates a ramp in time, and the approach will therefore be appropriate when the reaction is not diffusion-limited, through either a low binding probability or a finite reaction time (see Theory, and Figs. 4 and 5). This shortcut greatly facilitates study of the coupling reaction from G* to E*. Simulations under these conditions (see Fig. 9) confirm the earlier prediction in Eq. A8 of Lamb and Pugh (1992) that, when $G^*(t)$ is a ramp in time and the coupling reaction from G* to E* is diffusion limited (i.e., $p_{GE} = 1$), then $E^*(t)$ will also be a ramp.

RESULTS

Diffusion-limited activation of G* and E* (standard parameters)

The standard parameters for simulation are presented in Table 1; the values under Reaction Parameters approximate the diffusion limit to the rate of protein activation. The results of simulation with these parameters are shown in Fig. 3. The upper panel illustrates the superposition of traces for $G^*(t)$ and $E^*(t)$ from the first 20 simulations. This panel demonstrates the wide degree of variability obtained in successive simulations as a result of the finite number of activated molecules, and it shows that considerable averaging will always be needed to obtain a reliable estimate of the response.

Fig. 3 B plots the averages for $G^*(t)$ and $E^*(t)$ determined from a total of 100 such simulations. For $G^*(t)$ the average simulated response is virtually identical to the theoretical prediction of the diffusion limit in the continuous case (broken curve) obtained from Eq. 3 with $k_{RG} = \infty$ and $\rho_{RG} = 4.5$ nm. The close agreement here, between the simulation with $p_{RG} = 1$ and the continuous theory with k_{RG} infinite, results from having chosen the number of contacting pixels as $n_{contact} = 4$; see Fig. 2 B. As mentioned earlier, the ensemble variance had a time course very similar to the mean, for both G* and E*, although the variance was a little greater than the mean in this diffusion-limited case.

The average rates of activation for the two proteins (calculated over the interval 20–80 ms) were $\nu_G = 6370$ G* s^{-1} and $\nu_E = 4280$ E* s^{-1}, corresponding to a coupling efficiency c_{GE} from G* to E* of 67.2% ($= \nu_E/\nu_G$) at an E:G concentration ratio in this standard case of 1:10. Factors affecting the rates of activation and the efficiency of coupling will be investigated below.
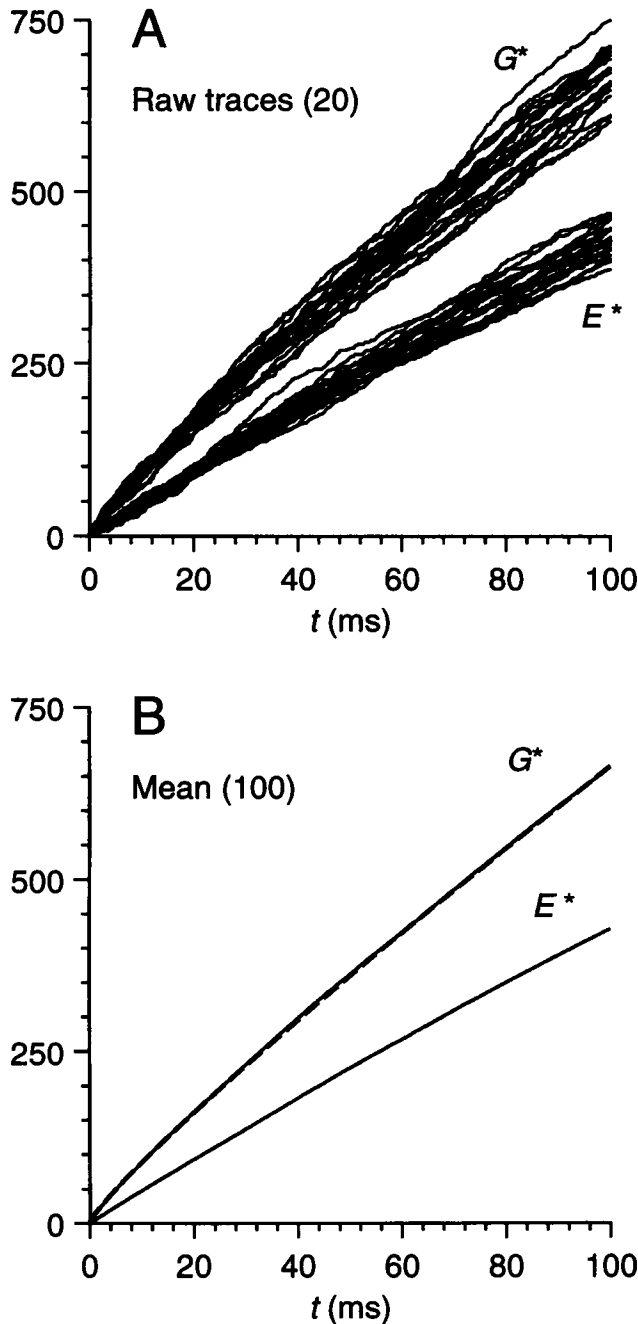
time for GTP binding to 0 ($\tau_{\mathrm{GTP}} = 0$); see Fig. 1 C and Table 1, Reaction Parameters. Nondiffusion-limited cases are illustrated in the next two figures, where p_{RG} was decreased below unity (Fig. 4) or τ_{GTP} was made finite (Fig. 5). The solid traces plot the averages of at least 20 simulations for each condition. The families of simulated responses in the two figures are quite similar, in that the curvature of the traces becomes progressively less pronounced as the rate of activation drops below the diffusion limit. Thus, as predicted earlier, the time course of G^* activation becomes more nearly linear with time (or ramp-like), when lateral diffusion is no longer the limiting factor.

In Fig. 4 the probability p_{RG} (that, upon contact, R* binds to G within the interval Δt) was varied from 100% to 1%, whereas in Fig. 5, τ_{GTP} (the mean time for GTP binding) was varied from 0 to 800 μs. Each of these parameters may alternatively be expressed in terms of a rate constant of binding (see Theory). k_{RG} ($\approx p_{\mathrm{RG}}/\Delta t$, see Eq. 7) is the rate constant with which R* binds to G upon contact, and in Fig. 4 it varied from ~500 −5 k s^{-1}. k_{GTP} (= τ_{GTP}^{-1}) is the rate constant of binding of GTP to the naked R*—G complex; in Fig. 5 it was infinite in the top trace and ranged from 20 to 1.25 k s^{-1} in the lower traces.
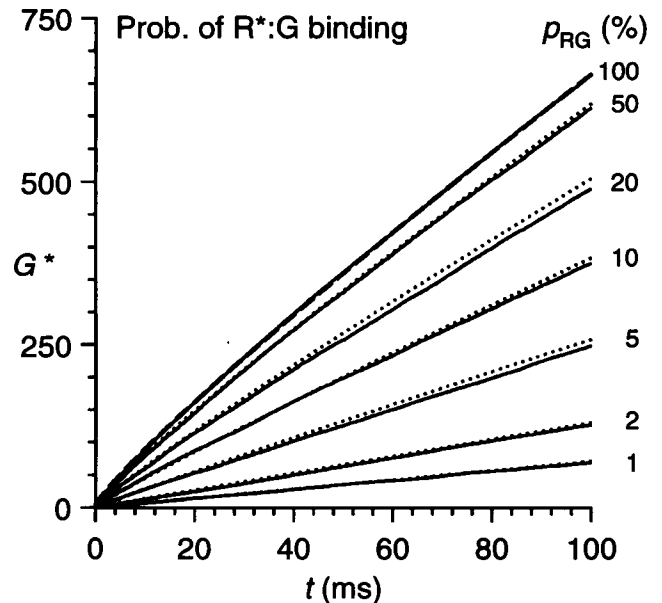
FIGURE 3   Simulations obtained with the standard parameters in Table 1, corresponding to the diffusion limit for activation. (A) Raw traces. The individual responses for $G^*(t)$ and $E^*(t)$ from the first 20 simulations are plotted. (B) Mean responses. The averages from 100 simulations are plotted as the solid traces. The broken trace (which is barely discernible) plots the diffusion limit for $G^*(t)$ in the continuous model, calculated from Eq. 3 with $k_{\mathrm{RG}} = \infty$ and $\tau_{\mathrm{GTP}} = 0$, and with collision radius $\rho_{\mathrm{RG}} = 4.5$ nm (i.e., as in Fig. 2B).

G* activation: finite rate constants

The approximation to the diffusion-limited rate of activation of G^* in Fig. 3 represents an extreme case obtained by setting the probability of R*:G binding to unity ($p_{\mathrm{RG}} = 1$) and the

FIGURE 4   Effect of finite probability of binding, p_{RG}, on the activation of G^* in the square lattice simulation. p_{RG} represents the probability that contact between an R* and a G leads to their binding during the simulation time step, Δt. In the continuous model the binding is more appropriately described by a rate constant, k_{RG} (see Eq. 1). The relationship between the rate constant k_{RG} and the probability p_{RG} is given in Eq. 7, and may be approximated by $k_{\mathrm{RG}} \approx p_{\mathrm{RG}}/\Delta t$. The solid traces plot the simulated responses, averaged from at least 20 simulations. The dotted traces plot the theoretical predictions for the square lattice, calculated from Eq. 3 with the equivalent values of ρ_{RG} and $2/a$ given by Eqs. 6 and 8. The broken trace plots the theoretical prediction for the continuous model, obtained from Eq. 3 with $k_{\mathrm{RG}} = \infty$, $\tau_{\mathrm{GTP}} = 0$ and $\rho_{\mathrm{RG}} = 4.5$ nm; this is the same trace as in Figs. 2 B, 3 B, and 5.
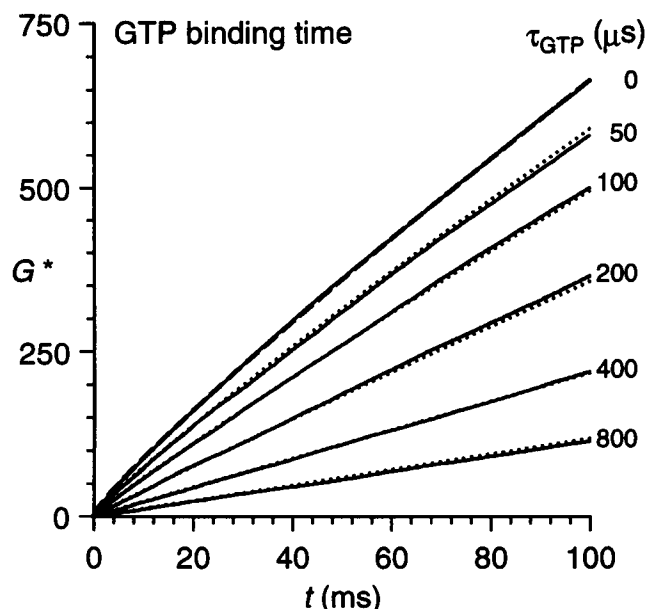
FIGURE 5   Effect of finite GTP binding time, τ_{GTP}, on the activation of G* in the square lattice simulation. Upon binding of R* to G, the bound GDP is assumed to dissociate instantaneously, but there is then a stochastic time with mean τ_{GTP} before a molecule of GTP binds, generating the active complex R*—G*$_{GTP}$ (see Fig. 1 C); the rate constant of GTP binding is k_{GTP} = τ_{GTP}^{-1}. The solid traces plot the simulated responses, averaged from at least 20 simulations. The dotted traces plot the theoretical predictions for the square lattice, calculated from Eq. 3c with the indicated values of τ_{GTP}. The broken trace again plots the theoretical prediction for the continuous model, obtained from Eq. 3 with $k_{RG} = \infty$, $\tau_{GTP} = 0$ and $\rho_{RG} = 4.5$ nm; this is the same trace as in Figs. 2 B, 3 B, and 4.

The second interpretation is that, for the conditions investigated, the continuous model and the square lattice are closely equivalent. The third interpretation is that, despite the difference in mechanisms involved between a finite probability p_{RG} for binding of R* to G and a finite time constant τ_{GTP} for binding of GTP to R*−G, the two processes have functionally similar effects in giving rise to a comparable time course for the activation of G*. For example, the traces with $p_{RG} = 20\%$ in Fig. 4 are almost identical to the traces with $\tau_{GTP} = 100$ μs in Fig. 5.

E* activation: dependence on the concentration of effector

The production of activated effector protein E* is examined in Fig. 6, as a function of the initial concentration C_E of inactive effector. For reference, the broken trace plots the activation of G* under the standard diffusion-limited conditions. The solid traces plot the activation of E* at the indicated concentrations of effector, from 25–750 μm^{-2} (corresponding to an E:G concentration ratio ranging from 1% to 30%). In these simulations the coupling was diffusion-limited, i.e., the G*:E binding probability, p_{GE}, was unity.

At the highest concentrations of effector, the activation of E* approaches that of G*, but at lower concentrations the rate of activation progressively drops. The coupling efficiency of the activation of E* by G*, denoted c_{GE}, was determined by taking the ratio ν_E/ν_G of the rates of activation of E* and G* (with the slopes determined over the interval 20–80 ms). This

In both figures the solid traces plot the stochastic simulations, whereas the dotted and broken traces plot the theoretical predictions obtained from Eq. 3. The single broken trace in each figure plots the diffusion-limited continuous theory, with $\rho_{RG} = 4.5$ nm (as in Figs. 2 B and 3). In Fig. 4 the dotted traces plot the predictions of the square lattice approximation, for the indicated values of the binding probability p_{RG}, with ρ_{RG} and $4D/k\rho^2$ obtained from Eqs. 6 and 8. In Fig. 5 the dotted lines plot the predictions of the square lattice approximation for finite GTP binding time, obtained from Eq. 3c, using the indicated values of τ_{GTP}.

The simulated responses and the theoretical traces agree quite well throughout the range of values of p_{RG} and τ_{GTP}. At the top of each figure, the three traces representing the diffusion limit are virtually indistinguishable from each other (and are identical in the two figures). Thus, what appears to be the top "trace" in each figure actually comprises three separate traces which almost superimpose: the simulation with $p_{RG} = 1$ and $\tau_{GTP} = 0$ (top solid trace), the continuous theory with $\rho_{RG} = 4.5$ nm (broken trace), and the square lattice theory with $p_{RG} = 1$ and $\tau_{GTP} = 0$ (top dotted trace, hidden beneath the other two traces).

The first interpretation of the results shown in Figs. 4 and 5 is that Eq. 3 (with the parameters from Eqs. 6 and 8) provides a good description of the simulated activation of G*, both in the diffusion-limited and nondiffusion-limited cases.
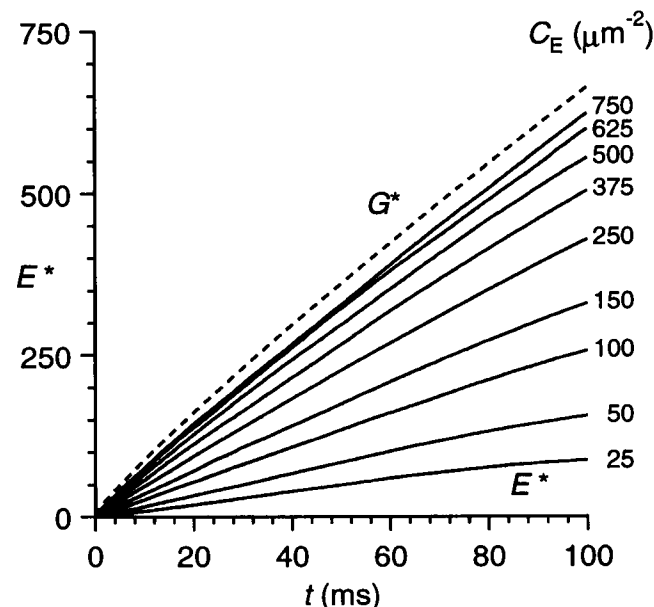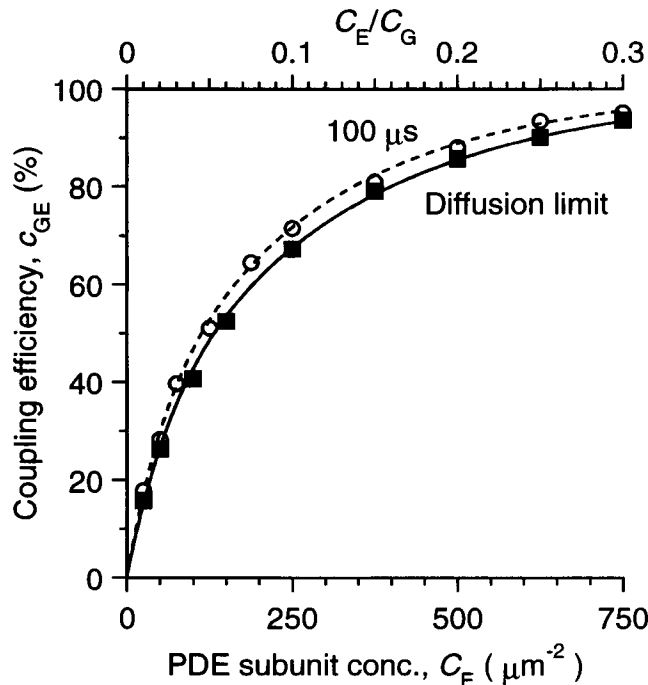

FIGURE 6   Activation of E* as a function of the concentration C_E of effector protein; all other parameters were set to the values in Table 1. For reference the broken trace plots the standard activation of G*, and the solid traces plot the simulated activation of E* for the indicated values of C_E. Activation in both cases corresponded to diffusion-limited conditions, with $p_{RG} = 1$ and $\tau_{GTP} = 0$ for G*, and with $p_{GE} = 1$ for the coupling from G* to E* (Table 1). At least 50 simulations were averaged to obtain each trace.

coupling efficiency c_{GE} has been plotted in Fig. 7 against the concentration of effector C_E (lower scale; also given as the concentration ratio C_E/C_G on the upper scale). For the filled symbols the rates of activation of G* and E* were both diffusion limited (data from Fig. 6), whereas for the open symbols the rate of G* activation was reduced below the diffusion limit through a finite GTP binding time constant of τ_{GTP} = 100 μs. The coupling efficiency was higher in the latter case because the rate ν_G of G* activation (which appears in the denominator) was then lower.

The results in Figs. 6 and 7 indicate that a reasonable coupling efficiency can be obtained with considerably less effector protein than G-protein present in the membrane. With an E:G concentration ratio of 1/10, the coupling efficiency exceeds 65% (even when the activation of G* is diffusion limited), and as the concentration of effector increases the coupling efficiency approaches unity.

Nevertheless, the coupling is not in fact as efficient as predicted by the earlier analytical approximation of Lamb
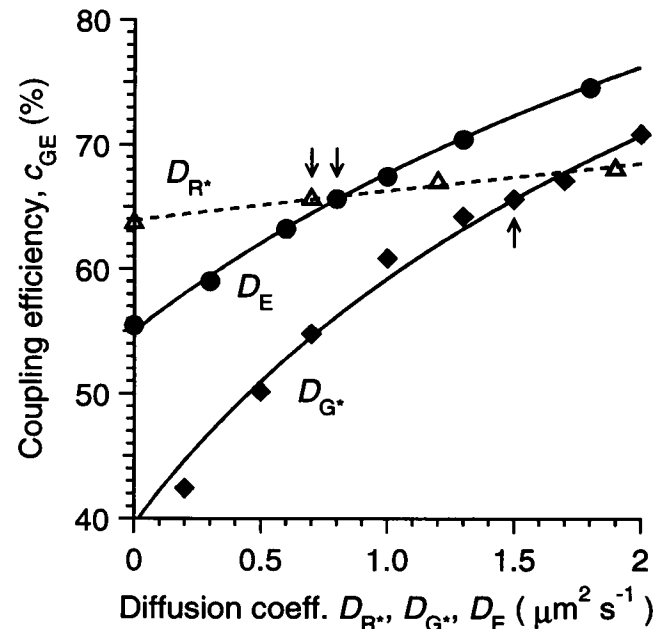
and Pugh (1992); see Eqs. 9a–c. That simplified model predicted that a coupling efficiency of 50% would be achieved at an E:G concentration ratio of ~3%, whereas the simulations indicate that a rather higher concentration ratio of ~6% is actually needed to obtain a 50% efficiency of coupling. The curves near the points in Fig. 7 plot a modified form of the earlier theory, in which the diffusion coefficients have been weighted; see Eq. 9d and Fig. 7 legend. The curves have the same shape as previously but are shifted by a factor of ~2 on the concentration axis.

E* activation: dependence of coupling on diffusion coefficients

The dependence of the coupling efficiency c_{GE} on the lateral diffusion coefficients is investigated in Fig. 8. The three sets of symbols indicate the effects of altering the lateral diffusion coefficients of the three species, R* (Δ), G* ($\blacklozenge$), and E ($\bullet$). To maintain a constant rate ν_G of G* activation when the diffusion coefficient of R* was increased, a corresponding decrease was made to the diffusion coefficient of the inactive G-protein; i.e., the sum $D_{R*} + D_G$ (equal to D in Eq. 3) was

FIGURE 7 Dependence of the coupling efficiency c_{GE} on the concentration C_E of effector protein, determined from results such as those in Fig. 6. The mean rates ν_G and ν_E of activation of G* and E* were determined over the interval 20–80 ms, and the coupling efficiency was then calculated as $c_{GE} = \nu_E/\nu_G$. The filled symbols are taken directly from Fig. 6, and represent the coupling efficiency when the activation of both G* and E* is diffusion limited. The open symbols are taken from corresponding results obtained with a GTP binding time of τ_{GTP} = 100 μs, i.e., when the activation of G* occurred at less than the diffusion limit, so that ν_G (which appears in the denominator of c_{GE}) was smaller. The curves were obtained from Eq. 9, using the weightings (see text) specified in the legend to Fig. 8, which gave D_{eff} = 1.4 μm^2 s^{-1}. The mean rates of activation of G* were ν_G = 6370 G* s^{-1} in the diffusion-limited case and 5270 G* s^{-1} with τ_{GTP} = 100 μs. (The open symbols were obtained from early simulations, where no correction was made to p_{move} and the "contacting" locations were defined as n_+ = 4, $n_\times$ = 3.)

FIGURE 8 Dependence of the coupling efficiency c_{GE} on the lateral diffusion coefficients of R* (Δ), G* ($\blacklozenge$), and E ($\bullet$). In the cases of G* and E, the respective lateral diffusion coefficients D_G and D_E alone were altered, and all other parameters were as set out in Table 1. However, when altering the diffusion coefficient of R*, D_{R*}, it seemed most appropriate to maintain a constant rate ν_G of activation of G*. Thus, when D_{R*} was varied, a complementary change was made to D_G, so that the sum $D_{R*} + D_G$ (equal to D in Eq. 3) was kept constant at 1.9 μm^2 s^{-1}. If D_G was not adjusted in this way, then the coupling efficiency actually declined with increasing D_{R*} because of the elevated rate ν_G of activation of G*. The arrows indicate the default values of the three diffusion coefficients. The curves fitted to the three sets of points were obtained from Eq. 9, a and b, with the effective diffusion coefficient D_{eff} in Eq. 9d weighted according to w_{R*} = 0.12, w_{G*} = 0.58 and w_E = 0.56. In these early simulations, no correction was made to p_{move} and the "contacting" locations were defined as n_+ = 4, $n_\times$ = 3.

kept constant at $1.9 \ \mu m^2 \ s^{-1}$. All other parameters were held at the values in Table 1 for the standard case.

Fig. 8 shows that the diffusion coefficient of R* has relatively little effect on the coupling efficiency of the subsequent activation of E* by G*. Indeed, if the value of D_{R*} *alone* is altered, without the compensating change in D_G, then the coupling efficiency actually drops as D_{R*} rises (not shown); this occurs because the rate ν_G (which appears in the denominator) increases, whereas the rate ν_E barely changes. The diffusion coefficients of G* and E have more marked effects on the coupling efficiency c_{GE}, and it is apparent that a low value of D_{G*} leads to a precipitous drop in coupling efficiency. The curves fitted to the results in Fig. 8 are from the modified form of the previous theory, in which the effectiveness of the three diffusion coefficients are individually weighted; see Eq. 9d. The weightings used were $w_{R*} = 0.12$, $w_{G*} = 0.58$ and $w_E = 0.56$, rather than each being unity as in the earlier simplified theory.

Taken together, the results of Figs. 6–8 show that efficient coupling from G* to E* can be obtained at surprisingly low E:G concentration ratios, and that the degree of coupling can be predicted accurately by a modified form of the theory of Lamb and Pugh (1992).

E* activation: finite rate constant of binding of G* to E

The kinetics of activation of E* are investigated in Fig. 9, upon systematic alteration of the probability p_{GE} of binding of G* to E. The values of the corresponding rate constant k_{GE} are given approximately by $k_{GE} \approx p_{GE}/\Delta t$ (analogous to Eq. 7), and for $p_{GE} = 1\%$ the value is $k_{GE} \approx 3000 \ s^{-1}$. The effect of a reduced binding probability is both to decrease slightly the rate of E* activation and also, very interestingly, to introduce a delay into its activation. The effective delay can be quantified by fitting a straight line to the later time course of $E*(t)$ and measuring its intercept with the abscissa (see dotted lines). For a binding probability of $p_{GE} = 1\%$ the effective delay t_{GE} is found to be approximately 12 ms, whereas for $p_{GE} = 0.1\%$ the delay increases to almost 60 ms.

In qualitative terms, the explanation for this behavior is the following. Molecules of G* are activated rampwise with time, but at first they cause little activation of E* because of the low probability of binding per collision. As a result the total quantity of available G* builds up steadily with time, and slowly these molecules spread outward spatially. At later times, G* molecules formed much earlier will have had many collisions with molecules of E, and binding will eventually occur at almost as high a rate as would have occurred if each collision had been successful.

The occurrence of an effective delay in the activation of E* may have a direct correlate in the response of real photoreceptors. From analysis of the electrical response of amphibian rods (which provide the basis for the parameters of Table 1), Lamb and Pugh (1992) reported that the total effective delay t_{eff}, from photon absorption to activation of E*, had a mean of 16 ms (range 10–20 ms) under voltage-
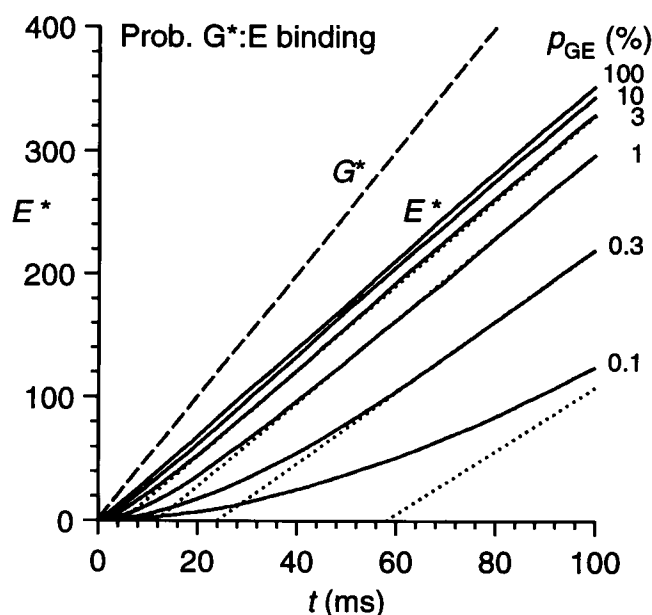

FIGURE 9 Activation of E* when the binding of G* to E occurs with finite probability p_{GE}. To speed the simulations, the shortcut described in the Methods section was employed, with G* being activated at a mean rate of 5000 G* s^{-1} (broken trace). The solid traces plot the simulated activation of E*, at the indicated values of p_{GE}; each trace is the average of at least 60 simulations. The parameter p_{GE} represents the probability that, upon contact between a G* and an E, the two bind during the simulation time increment, $\Delta t = 2.5 \ \mu s$. In the continuous model the binding of G* to E is more appropriately expressed in terms of a rate constant k_{GE}, given by an equation analogous to Eq. 7 for k_{RG}. The dotted traces are straight lines fitted to the final ramplike rise of $E*(t)$; to enable fitting of the bottom response (for $p_{GE} = 0.1\%$) the simulation time in that case was extended to $t_{max} = 200$ ms (not shown). The intercepts of the dotted lines with the abscissa give the effective delay time t_{GE} of the coupling from G* to E.

clamped conditions and at 22°C; this represents an upper limit for the coupling delay from G* to E* activation. In light-scattering experiments Heck and Hofmann (1993) reported a delay of 5–10 ms between activation of G* and E*. A plausible explanation for an appreciable part of these experimentally reported delays would be a finite rate constant of binding of G* to E.

Inspection of Fig. 9 shows that the traces for $E*(t)$ remain approximately parallel until p_{GE} drops below 1%. This indicates that the coupling efficiency c_{GE} is only weakly dependent on the rate constant of binding, and that it remains quite high until k_{GE} drops below about 3000 s^{-1}. Similarly, the coupling delay t_{GE} begins to increase significantly only when k_{GE} drops below roughly the same level.

DISCUSSION

Phototransduction serves as a model G-protein system, because the important physical parameters of the cascade (such as the concentrations and lateral diffusion coefficients of the protein molecules) are known accurately, and because the molecular reactions of activation are particularly well understood. The least well understood aspects of phototransduction relate to the inactivation reactions that underlie recovery of the light response. Although a number of

inactivation processes have been described in general terms, there remains uncertainty about the details and the relative importance of the different reactions, and the quantitative parameters of inactivation have not yet been determined in vivo. For these reasons, as well as for rendering the mathematical analysis tractable, it is at present necessary to restrict quantitative treatment to the activation steps in transduction.

In this paper the process of activation in the G-protein cascade of phototransduction has been studied by stochastic simulation. The simulations confirm the main predictions of the previous simplified analytical approach of Lamb and Pugh (1992) and extend that treatment by dealing with nondiffusion-limited conditions and providing a corrected description of the coupling from G* to E*.

Activation of G*

Activation of the G-protein to G* has been simulated under diffusion-limited conditions (i.e., when the rate of reaction is determined by the rate of molecular collisions occurring as a result of two-dimensional lateral diffusion of the protein molecules), as well as when the probability p_{RG} of binding of R* to G is less than unity, or when the time τ_{GTP} to bind GTP is finite. Under all of these conditions the rate of activation is well described by Eq. 3. Although Eq. 3 may appear complicated, and despite its inclusion of a logarithmic time dependence, the equation in fact predicts a rate of G* activation, which is roughly constant. The greatest deviation from a constant rate of activation occurs in the diffusion limit, but inspection of Fig. 3 (or mathematical analysis of Eq. 3) shows that even in this case the curvature is relatively minor (see Lamb and Pugh, 1992). The diffusion-limited rate is then given approximately by the simple expression

$$\nu_G \approx 1.3 \, (D_{R*} + D_G)C_G. \tag{10}$$

When the probability p_{RG} of R*:G binding decreases, or the time τ_{GTP} for GTP binding increases, the rate of G* activation drops and the curvature of the traces becomes less. Thus, especially in nondiffusion-limited cases, the activation of G* is described to a very good approximation by a ramp in time.

Delayed ramp activation of E*

The ramplike activation of G* is significant because the previous theoretical analysis of Lamb and Pugh (1992) predicted that a constant rate of G* activation would lead to a constant rate of E* activation, in the case of diffusion-limited coupling from G* to E* (see Eq. A8, Lamb and Pugh, 1992). That theoretical prediction has been verified in the present simulations (see Fig. 9, uppermost solid trace).

Thus, when the coupling from G* to E* is diffusion limited, then the activation of E* is simply a scaled version of the activation of G*; i.e., $G*(t)$ ramps with time, with zero delay. The effect of lowering the probability p_{GE} of binding of G* to E (thereby taking the coupling reaction below the diffusion limit) is to introduce a delay into the time course

of E* activation while causing relatively little change in the efficiency of coupling (lower traces in Fig. 9). A delay of just this kind seems to occur in transduction both in intact rod photoreceptors where the delay is about 15 ms at room temperature (Lamb and Pugh, 1992) and in reconstituted disc membranes where a delay of 5–10 ms has been reported (Heck and Hofmann, 1993). A plausible cause of this experimentally observed delay in E* activation would be a low probability p_{GE} of binding of G* to E. Examples of the kind of mechanism that could give rise to a low rate constant of binding k_{GE} (equivalent to a low probability of binding p_{GE}) would include the need for precise molecular orientation before binding occurs, or the existence of an energy barrier to be overcome upon binding.

Relevance of the simulations to the photoresponse

The simulations show that, over a wide range of the reaction parameters p_{RG}, τ_{GTP}, and p_{GE}, the number of activated molecules of E* *ramps* with time after a brief flash of light (provided that inactivation reactions are ignored). This ramping is precisely the form of $E*(t)$ needed to explain the rising phase of the electrical response of vertebrate photoreceptors (Lamb and Pugh, 1992); it enables the activation phase of the light response to be explained quantitatively over an extremely wide range of light intensities.

The values adopted here for the lateral diffusion coefficients of the proteins are the best current estimates applicable to amphibian rods at room temperature; see Pugh and Lamb (1993). However, even if these values are in error, the form of the predictions should still be accurate. Adopting these values for the diffusion coefficients, the simulations show that at the diffusion limit E* can be activated at around 4000 catalytic subunits s^{-1} per R*. Thus the simulations confirm in a direct way our previous theoretical interpretation that the reactions of the G-protein cascade can occur rapidly enough, simply as a result of lateral diffusion of proteins at the surface of the disc membrane, to account fully for the gain and speed of phototransduction. Therefore the simulations confirm the finding of Lamb and Pugh (1992) that there is no need to invoke an aqueous path for diffusion of G*$_{GTP}$ (i.e., movement of G*$_{GTP}$ into the cytoplasm) to explain the kinetics of phototransduction. In line with this conclusion, evidence has recently been obtained that G*$_{GTP}$ binds tightly to the membrane after activation in vivo (Catty et al., 1992; see Hofmann and Heck, 1994), and it is therefore unlikely that any appreciable fraction moves into solution over the time scale of activation of the light response.

Factors affecting the coupling efficiency from G* to E*

The activation of effector protein to E* has been studied as a function of the concentration C_E of effector in the membrane, and as a function of the lateral diffusion coefficients of the three proteins. The effectiveness of coupling from G*

to E* can be characterized by the ratio of the rates of activation, termed the coupling efficiency, $c_{GE} = \nu_E/\nu_G$. As predicted by the previous simplified analysis, a reasonable efficiency of coupling is achieved at a surprisingly low concentration ratio of effector protein to G-protein in the membrane.

However, the simulations exposed a quantitative shortcoming of the previous approximate analysis, and indicated that the required concentration ratio is roughly double that predicted by the simplified theory. Thus, to achieve a coupling efficiency of $c_{GE} = 50\%$ with parameters applicable to the amphibian rod photoreceptor, the required effector protein to G-protein concentration ratio is $C_E/C_G \approx 6\%$ rather than about 3% according to the previous analysis. Nevertheless, the required concentration ratio, of about 1/16, is still quite low. Furthermore, it must be remembered that in the case of the photoreceptor the concentration C_E is expressed in terms of PDE catalytic subunits, of which there are two per PDE holomer. Thus the concentration of PDE molecules needed to achieve a coupling efficiency of 50% is only about 3% of the concentration of G-protein molecules; i.e., for $C_G = 2500 \ \mu m^{-2}$ the required effector subunit concentration is $C_E \approx 150 \ \mu m^{-2}$, corresponding to about 75 PDE molecules/μm^2.

The most recent biochemical measurements of the protein content of amphibian rod photoreceptors indicate that the holo-PDE is in the ratio to rhodopsin of approximately 1 PDE : 270 R (Dumke et al., 1994), whereas the G-protein is established as being in the ratio 1 G:10 R (Hamm and Bownds, 1986). These ratios correspond to protein concentrations of $C_G = 2500$ G-proteins/μm^2 (as in Table 1) and 93 PDE holomers/μm^2, or $C_E = 185$ PDE catalytic subunits/μm^2. Inspection of Fig. 7 indicates that this PDE concentration (with the other parameters at their standard values) should correspond to a coupling efficiency of about 59% if the activation of G* is diffusion limited and about 64% if the activation of G* is slowed by a GTP binding time with a mean of 100 μs. If the rate of G* activation were slower than calculated using the parameter values in Table 1, then the efficiency of coupling to E* would be higher still.

Optimization of protein concentrations

One can reasonably expect the protein concentrations in the outer segment to have been "optimized" for the purposes of transduction. Some of the criteria for optimization are immediately apparent, but at this stage there are presumably other criteria yet to be determined.

For the purpose of maximizing the gain of transduction, the concentration of each of the three protein species should be high. A higher rhodopsin concentration will lead to the absorption of a greater proportion of the incident photons; a higher G-protein concentration will lead to a greater rate of activation of G* and hence to a higher gain of transduction; a higher PDE concentration will lead to a greater coupling efficiency and hence also to a higher gain of transduction.

There are, however, inevitable "costs" associated with high protein concentrations, which conflict with the purpose of maximizing the transduction gain, or which cause other drawbacks. A very high total concentration of protein will lead to a reduction in the fluidity of the disc membrane (Peters and Cherry, 1982) and thereby to a reduction in each of the lateral diffusion coefficients. This will lower the rates of activation of G* and E* and thereby lower the gain of transduction. It would seem that this consideration will be of greatest importance in determining the optimal concentration of rhodopsin, as the quantity of the photopigment far outweighs that of the other proteins ($\sim$1 R : 0.1 G : 0.004 PDE).

Each of the three proteins will be subject to the disadvantage that, even in darkness, its presence will inevitably lead to some residual level of activation, and therefore to a phenomenon broadly equivalent to a steady background of light; i.e., it will cause an "equivalent background" of the kind postulated originally by Stiles and Crawford (1932). Such an equivalent background will be disadvantageous to the organism, in that it will elevate the threshold for stimulus detection in the overall visual system; for reviews see Barlow (1972) and Pugh (1988). At the level of the photoreceptor, the disadvantage of an equivalent background is that it will reduce the magnitude of the circulating current in darkness (the dark current). It is also possible that the presence of a continual equivalent background at an excessive level could lead to degeneration of the photoreceptor outer segments (Fain and Lisman, 1993).

Rhodopsin exhibits spontaneous thermal activation to R* (Baylor et al., 1980, 1984), although at the exceedingly low rate of $\sim 10^{-11}$ R* s^{-1}/rhodopsin at room temperature. Likewise, the G-protein will be subject to thermal activation to G*. For example, the G_{GDP} may spontaneously lose its bound GDP; alternatively, the GDP may occasionally be converted back to GTP as a result of the inevitable slight degree of reversibility of the inactivation reaction that hydrolyzes the terminal phosphate of G*$_{GTP}$. Similarly, the "inactive" PDE will inevitably exhibit residual hydrolytic activity in darkness even in the absence of G*. It is unlikely that the γ subunits could totally inhibit the hydrolytic activity of the PDE when they are present, but in any case these γ subunits will exhibit finite binding constants so that there must be a finite probability that they will dissociate from the α,β subunits and thereby relieve the inhibition (see Wensel and Stryer, 1986).

Hence, in optimizing transduction, it would be beneficial to increase the concentration of the G-protein until a region of diminishing returns was reached in the rate of activation of the effector to E*. This might occur upon approaching a limit to the rate of activation of G*, or when the coupling from G* to E* could no longer keep up with ν_G. Thus, there would be no advantage in having a G-protein concentration so high that the rate of activation ν_G became limited by k_{GTP}, nor would there be any advantage in having ν_G so high that the coupling efficiency c_{GE} from G* to E* dropped significantly. In either case the high concentration of G-protein would be disadvantageous in contributing to spontaneous

activation of G* in darkness (i.e., producing an equivalent background) without significantly aiding transduction.

It would similarly be worthwhile to increase the concentration of the PDE but again only until the advantages were outweighed by the disadvantages. At high concentrations of PDE, very little improvement is gained in the rate of activation of E* by any further increase in concentration, because the incremental slope in Fig. 7 becomes small. But a high PDE concentration is disadvantageous in causing an increased resting rate of hydrolysis of cyclic GMP, raising the equivalent background and unnecessarily suppressing the circulating current or costing energy in maintaining a higher basal guanylate cyclase rate.

This optimization problem is one in which a factor (e.g., protein concentration) leads to advantage (e.g., increased gain) in a saturating manner, and to disadvantage (e.g., equivalent light) in a manner that causes the noise variance to increase in a linear manner. In this class of optimization problem, it is possible to show that the optimal signal-to-noise ratio occurs at between 50 and 100% of the maximum possible output level, depending on the baseline level of noise variance. Typically one might expect the optimum output level to be in the range 60–80% of the maximal output. Thus it would be reasonable to expect that activation of G* would proceed at roughly 60–80% of the diffusion limit, and that coupling from G* to E* would occur with an efficiency of around 60–80%. Lower values would lead to an inadequate gain of transduction, whereas higher values would lead to an excessive equivalent background in darkness with relatively little circulating current in the photoreceptors and with elevated threshold in the visual system.

Inspection of Fig. 7 would therefore suggest that the optimum PDE concentration should be ~200–400 subunits μm^{-2}, or 100–200 holomers μm^{-2}. It is satisfying that the most recent estimates of native PDE concentration correspond quite closely to this, at just under 100 holomers μm^{-2} (Dumke et al., 1994). This result is consistent with the idea that the quantity of PDE has been optimized, in the sense that there is just sufficient PDE present to achieve a respectable efficiency of coupling, but there is no more than that.

Relative expense of the proteins

Although it is reasonably straightforward from the approach above to predict the optimal quantity of PDE in the case of a given amount of G-protein, it is difficult to go further. To predict the optimal concentration of each of the protein molecules, it will be necessary to express all of the advantages and disadvantages of the proteins in quantitative terms.

The high concentration of photopigment in the cell can be viewed as an indication that native rhodopsin is relatively innocuous, exhibiting little in the way of disadvantage in comparison with the other proteins. The very much lower concentration of PDE suggests that the "expense" (or the disadvantage relative to the advantage) of the PDE may be much greater than that of the other two proteins. This would be consistent with the notion that the spontaneous activity per molecule (or the

"equivalent background" per molecule) is much greater for the PDE than for the G-protein or rhodopsin.

Even so, the residual activity of the PDE is quite low. The resting hydrolytic rate constant of the PDE in darkness in intact amphibian rods has been estimated as ~0.5 s^{-1} from electrophysiological experiments (Hodgkin and Nunn, 1988), whereas the fully activated hydrolytic rate constant in bright light has been estimated as ~300 s^{-1} from electrophysiological experiments (Lamb and Pugh, 1992) and as ~1000 s^{-1} from biochemical experiments (Dumke et al., 1994). Thus the maximal PDE activity is ~600–2000 times greater than the resting PDE activity. Note, however, that this represents a lower limit for the inhibition ratio per se, given that the resting PDE activity in vivo will inevitably include a contribution from any residual R* and G* activity. Other estimates of the PDE inhibition ratio are at least 1700 (Wensel and Stryer, 1986), and at least 300 (Dumke et al., 1994).

The organization of the phototransduction cascade may be viewed in the following terms. The receptor protein rhodopsin is present at a very high concentration, but it has an extremely high energy barrier that minimizes spontaneous activation of the high-gain catalytic cascade of reactions. The G-protein has a smaller barrier to spontaneous activation, and is present at a lower concentration. The effector protein PDE has an even smaller barrier to spontaneous activation, and is present at the lowest concentration.

Inactivation reactions

Because of the present uncertainty about the reactions involved in inactivation of the photoresponse, the analysis in this paper has been restricted to the activation steps of transduction. However, as soon as the turnoff reactions are thoroughly understood and properly quantified, it will be straightforward to include them in a modified version of the "WALK" program.

REFERENCES

Barlow, H. B. 1972. Dark and light adaptation: psychophysics. *In* Handbook of Sensory Physiology, Vol. VII/4. D. Jameson and L. M. Hurvich, editors. Springer, Berlin. 1–28.

Baylor, D. A., G. Matthews, and K.-W. Yau. 1980. Two components of electrical dark noise in toad retinal rod outer segments. *J. Physiol.* 309: 591–621.

Baylor, D. A., B. J. Nunn, and J. L. Schnapf. 1984. The photocurrent, noise and spectral sensitivity of rods of the monkey *Macaca fascicularis*. *J. Physiol.* 357:575–607.

Berg, H. C. 1983. Random Walks in Biology. Princeton University Press, Princeton. 142 pp.

Catty, P., C. Pfister, F. Bruckert, and P. Deterre. 1992. The cGMP phosphodiesterase-transducin complex of retinal rods. Membrane binding and subunits interactions. *J. Biol. Chem.* 267:19489–19493.

Dumke, C. L., V. Y. Arshavsky, P. D. Calvert, M. D. Bownds, and E. N. Pugh Jr. 1994. Rod outer segment structure influences the apparent kinetic parameters of cyclic GMP phosphodiesterase. *J. Gen. Physiol.* 103: 1071–1098.

Fain, G. L., and J. E. Lisman. 1993. Photoreceptor degeneration in vitamin A deprivation and retinitis pigmentosa: the equivalent light hypothesis. *Exp. Eye Res.* 57:335–340.

Hamm, H. E., and M. D. Bownds. 1986. Protein complement of rod outer segments of frog retina. *Biochem.* 25:4512–4523.

Heck, M., and K. P. Hofmann. 1993. G-protein-effector coupling: a real-time light-scattering assay for transducin-phosphodiesterase interaction. *Biochem.* 32:8220–8227.

Hodgkin, A. L., and B. J. Nunn. 1988. Control of light-sensitive current in salamander rods. *J. Physiol.* 403:439–471.

Hofmann, K. P., and M. Heck. 1994. Light-induced protein-protein interactions on the rod photoreceptor disc membrane. *In* Biomembranes II. A. G. Lee, editor. JAI Press. In press.

Hofmann, K. P., and M. Kahlert. 1992. The activation of transducin: studies on its mechanism and modulation. *In* Signal Transduction in Photoreceptor Cells. P. A. Hargrave, K. P. Hofmann, and U. B. Kaupp, editors. Springer, Berlin. 71–102.

Jaeger, J. C. 1942. Heat flow in the region bounded internally by a circular cylinder. *Proc. R. Soc. Edinb. A Math. Phys. Sci.* 61:223–228.

Lamb, T. D. 1993. Gain and kinetics of activation in G protein cascades. *J. Physiol.* 459:344P.

Lamb, T. D., and E. N. Pugh Jr. 1992. A quantitative account of the activation steps involved in phototransduction in amphibian photoreceptors. *J. Physiol.* 449:719–757.

Peters, R., and R. J. Cherry. 1982. Lateral and rotational diffusion of bacteriorhodopsin in lipid bilayers: experimental test of the Saffman-Delbrück equations. *Proc. Natl Acad. Sci. USA.* 79:4317–4321.

Pugh, E. N. Jr. 1988. Vision: physics and retinal physiology. *In* Steven's Handbook of Experimental Psychology, Vol. 1, Perception and Motivation. R. C. Atkinson, R. J. Herrnstein, G. Lindzey, and E. D. Luce, editors. John Wiley, New York. 75–163.

Pugh, E. N. Jr., and T. D. Lamb. 1993. Amplification and kinetics of the activation steps in phototransduction. *Biochim. Biophys. Acta.* 1141:111–149.

Razi Naqvi, K. 1974. Diffusion-controlled reactions in two-dimensional fluids: discussion of measurements of lateral diffusion of lipids in biological membranes. *Chem. Phys. Lett.* 28:280–284.

Stiles, W. S., and B. H. Crawford. 1932. Equivalent adaptational levels in localized retinal areas. *In* Report of a Joint Discussion on Vision. Physical Society of London. Cambridge University Press, Cambridge. 194–211. *Reprinted in* Stiles, W. S. 1978. Mechanisms of Colour Vision. Academic Press, London. 298 pp.

Torney, D. C., T. Warnock, M. A. McCloskey, M. Dembo, and M.-M. Poo. 1987. Rates of chemical reactions taking place in two dimensions. *Comments Mol. Cell. Biophys.* 4:281–303.

Wensel, T. G., and L. Stryer. 1986. Reciprocal control of retinal rod cyclic GMP phosphodiesterase by its gamma subunit and transducin. *Proteins Struct. Func. Genet.* 1:90–99.